FEDSM2020-13298

Numerical Investigation and Performance Characterization of Oscillating Foil Energy Harvesting

James Pannell and D. Keith Walters

School of Aerospace and Mechanical Engineering
University of Oklahoma
Norman, Oklahoma, USA

ABSTRACT

Oscillating foil energy harvesting devices are increasingly being considered as a sustainable energy alternative, especially in rivers and tidal areas. This paper applies CFD to an oscillating foil power generation device in order to explore the effects of pitching amplitude, the ratio of heaving amplitude to chord length, and the reduced frequency to the energy harvesting efficiency. Ansys Fluent 17.2 was used for this study, and the results are compared to experimental results that have been previously documented in the open literature. Configurations examined included pitching amplitudes of 65, 70, 75, and 80 degrees; heaving ratios of 0.4, 0.6, and 0.8; and reduced frequencies of 0.1, 0.12, 0.14, and 0.16. Results seems to indicate that the optimal reduced frequency is related to the heaving ratio, with the pitching amplitude only creating slight variations in the power produced by the foil. In the data, configurations with a heaving ratio of 0.4 have highest efficiency at reduced frequencies of either 0.14 or 0.16, but efficiency remains high at both points, which indicates the possibility of a peak in between the two points. Configurations with heaving ratio of 0.6 peak at reduced frequency 0.14 with a significant drop off at reduced frequency of 0.16. Finally, configurations with a heaving ratio of 0.8 show a peak at 0.12 reduced frequency and a significant drop at 0.14 and 0.16. These results suggest that OFEH devices can be effectively optimized for different and potentially varying operating conditions that may be encountered during practical implementation of OFEH technology.

INTRODUCTION

The application of oscillating foil energy harvesting (OFEH) devices has increasingly been considered as a sustainable energy alternative, especially in rivers and tidal areas. Such devices can potentially avoid the centrifugal stresses and large translational tip speeds associated with traditional turbine energy harvesters

[1]. Limiting these effects allows for the reduction of cost by needing fewer high-performance materials, and reduces the potential environmental impacts of noise and, in the case of wind turbines, threat of birds physically striking the turbine blade. In order to achieve high power output in OFEH devices, it is necessary to understand the effects of various parameters on the efficiency of the device.

There are several parameters influencing the performance of an OFEH device. In this study, three dimensionless operating conditions were examined: reduced frequency (k), normalized heaving amplitude (h_{θ}) , and pitching amplitude (θ) , defined as:

$$k = \frac{fc}{U_{\infty}} \tag{1}$$

$$h_0 = \frac{h}{c} \tag{2}$$

where f is the frequency of oscillation, c is the airfoil chord length, U_{∞} is the freestream velocity, and h is the maximum amplitude of heaving, i.e. the maximum displacement of the airfoil centroid in the vertical direction during the oscillation cycle. Pitching amplitude is the maximum rotation of the airfoil from the horizontal position during the oscillation cycle. OFEH performance is characterized by the power output, P, which can be defined instantaneously or integrated over one or more cycles to yield cycle-averaged power, \bar{P} . In actual operation, the electrical power delivered by the OFEH depends on electrical and mechanical system losses. When considering the fluid dynamic performance, power is assumed to represent the power delivered to the foil by the flowing water. The efficiency, η , of the device can be defined as the power output normalized by the total available power for the water that would otherwise flow through the area, A, swept by the oscillating foil:

$$\eta = \frac{\bar{P}}{\frac{1}{2}\rho A U_{\infty}^3} \tag{3}$$

Previous computational work based on unsteady, 2-D laminar simulations in Ansys FLUENT has indicated that the optimum efficiency range for simple periodic (sinusoidal) oscillation is k = 0.12 to 0.16, $h_0 = 0.5$ to 1.0, and $\theta = 75^{\circ}$ to 85° [2]. It was noted that many of the most efficient cases studied involve large amounts of leading-edge vortex shedding. Experimental results using wind tunnel testing have indicated a maximum efficiency of approximately 25% at a reduced frequency of 0.14 [3]. This experimental data was found using a foil of finite length, while the simulations conducted in this study and in most previous work have assumed an idealized 2-D flow to evaluate computational efficiency. Other studies of OFEH devices have investigated the performance of non-sinusoidal foil pitching motions and found an increase in efficiency as compared to the sinusoidal pitching motion. Efficiencies of up to 41% were found in some 2-D simulations of non-sinusoidal pitching motions [4].

The objective of the present study is to apply computational fluid dynamics (CFD) to various cases in the operational range of reduced frequency (k) from 0.1 to 0.16, heaving amplitude (h_0) from 0.4 to 0.8, and pitching amplitude (θ) from 65° to 80°, and to identify trends in efficiency as a function of these parameters.

NUMERICAL METHODS

Numerical simulation of flow over the oscillating foil was conducted using unsteady two-dimensional finite-volume computational fluid dynamics (CFD) simulation in Ansys Fluent v. 17.2. The pressure-based formulation was used. A second order upwind scheme was used for the convective terms of the momentum equations. Face mass fluxes were computed using a momentum interpolation method similar to Rhie-Chow interpolation. The pressure terms of each model were discretized using a standard scheme in which the face pressure was obtained from an average of the pressure values in neighboring cells. The SIMPLE scheme was used for pressure velocity coupling. Fluid properties were assumed to be constant and equal to those for liquid water at standard atmospheric pressure and temperature.

The transient formulation employed was the second-order implicit (three-point backward difference) scheme. For unsteady computations using an implicit time-stepping scheme, convergence of all flow variables should occur at each time step. In the present study, convergence was confirmed by ensuring that the RMS momentum equation residual was reduced by at least three orders of magnitude during each time step. This was further verified by ensuring that forces and moments acting on the foil converged to numerically steady values during each time step. As discussed below, several different time step sizes were investigated to determine their effect on solution accuracy.

The moving foil was simulated using the arbitrary Lagrangian-Eulerian (ALE) formulation in Fluent. The foil represented the only solid surface boundary in the simulation, i.e.

the foil was assumed to be oscillating in a uniform freestream. For this reason, the entire mesh followed the prescribed foil motion and no deformation or interface matching between moving and stationary domains was necessary.

All simulations were run with a Reynolds number less than 20,000 based on foil chord length and freestream velocity. It was therefore assumed that flow was laminar. However, a selection of cases were additionally run using k- ω [5] and k-k- ω [6] turbulence models as a comparison, based on the assumption that transition to turbulent flow could occur in separated flow regions. Results in terms of overall energy extraction efficiency are shown in Table 1. Based on these results, it was determined that the variation between the turbulence and laminar simulations was relatively small, and no clear advantage could be deduced for using turbulence modeling in this Reynolds number range. Since the use of turbulent models also significantly increased the computational cost of simulations, the laminar simulation method was used for all of the results presented in the remainder of the paper.

Table 1. Predicted efficiency using different modeling methods for three sets of operating conditions

Method	Operating Conditions			
	k = 0.1	k = 0.12	k = 0.14	
	$h_{\theta} = 0.4$ $\theta = 70$	$h_{\theta} = 0.6$ $\theta = 70$	$h_{\theta} = 0.6$ $\theta = 65$	
Laminar	0.23	0.30	0.29	
k-ω	0.25	0.30	0.27	
k-kl-ω	0.25	0.28	0.27	

SIMULATION SETUP Computational Domain

The computational domain considered in this paper models a 2D finite-thickness plate with elliptical leading and trailing edges, oscillating in a uniform freestream flow. The computational domain is circular with radius 2.5 meters centered on the centroid of the plate. The plate itself is a flat plate with a chord of 12.5 cm, thickness of 0.625 cm, leading and trailing edge ellipses with a 5:1 ratio of major to minor axis lengths. The computational domain is shown below in Figure 1. The plate was treated as a no-slip wall for boundary conditions, and uniform velocity components and pressure were specified on the far field boundary.

To capture the heaving and pitching behavior of the foil, a user defined function (UDF) was used to define a mesh motion in the cell zone conditions for the fluid zone. All of the motions considered in this paper have heaving and pitching 90° out of phase.

Grid

The grid used is a structured grid. Finer cells were used in the near wall region to resolve the boundary layer and cells gradually increased in size towards the far field boundary to reduce computational cost. The grid contained 84,160 nodes and 83,840 cells. Simulations were run for 30 seconds of physical time with a step size of 10⁻³ seconds to ensure simulations converged.

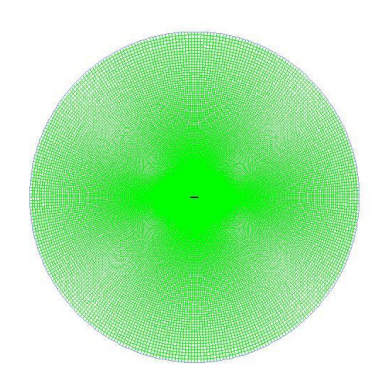


Figure 1. 2D domain and computational mesh.

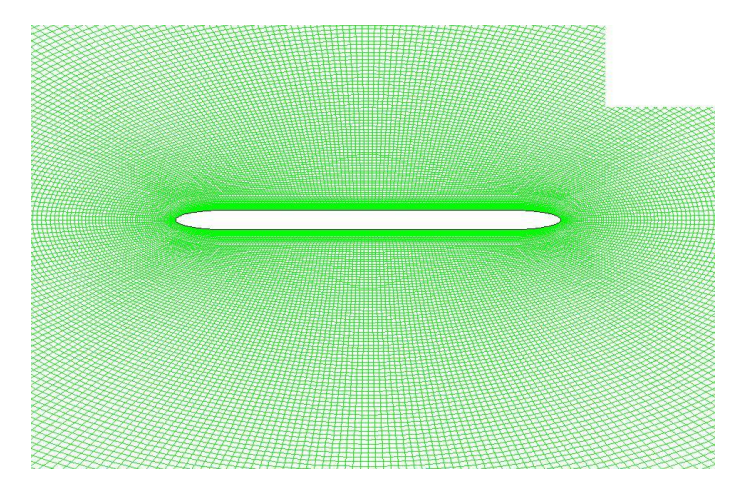


Figure 2. Illustration of computational mesh near the foil

EFFECT OF MESH RESOLUTION AND TIME-STEP SIZE

The effect of both mesh resolution and time-step size on the simulation results was investigated to verify that the selected mesh and time-step size was sufficient to identify the correct trends in OFEH performance. Using the initial mesh, an investigation into simulation sensitivity to time-step size has been performed. Three test cases were selected, with different heaving and pitching amplitudes and reduced frequencies. Three different time-step sizes were used: $\Delta t = 0.001s$, 0.0032s, and 0.0001s. Results are shown in terms of efficiency in Figure 3. For each case, the predicted efficiency is reduced as the timestep size is reduced. It is also not apparent that the results are yet independent to time-step size even at the smallest value of 0.0001s. However, results do seem to indicate that the trends in the results are maintained for all time-step sizes. That is, if one case is more efficient than another at one time-step size, this relationship will hold as the time-step size is reduced. For this reason, and in the interest of computational efficiency, all results

presented in this paper were obtained using a time-step size of $\Delta t = 0.001s$.

For the mesh resolution study, a refined mesh was created with identical topology and relative cell distribution as that shown in Figure 2, but with an increase in cell count from 84K to 335K cells. For the case with reduced frequency of 0.12, heaving amplitude of 0.6c, and pitching amplitude of 75°, efficiency was calculated to be 0.298 with a grid of 84,160 nodes, and 0.304 for 336000 nodes. This is a difference of approximately 2%, and therefore the baseline mesh was assumed to be sufficiently well resolved for the purposes of this study.

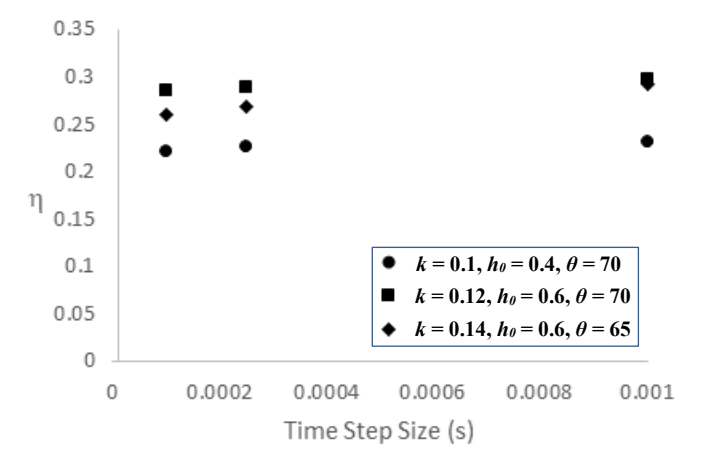


Figure 3. Efficiencies of select cases calculated using three different time-step sizes ranging from 0.0001 s to 0.001 s.

RESULTS AND DISCUSSION

Numerical simulation results for all cases are presented in this section. Simulations were run at Reynolds numbers varying from 6,685 to 17,828. For all cases, the frequency of both pitching and heaving was f = 1 Hz. The reduced frequency was varied by changing the freestream velocity.

The cases were each simulated for 30 seconds of physical time and the lift force (F_y) and pitching moment (M_z) acting on the foil were recorded at every time step. Using this data, the instantaneous power due to heaving and pitching, respectively, were calculated using the following:

$$P_h(t) = F_{\nu}V_{\nu} \tag{4}$$

$$P_p(t) = M_z \omega_z \tag{5}$$

where V_y is the vertical velocity of the foil and ω_z is the pitching rate. The total instantaneous power is the sum of these two components:

$$P = P_h + P_h \tag{6}$$

Figures 4-11 show the time-varying power developed buy the oscillating foil over one representative cycle, for each set of operating conditions investigated. Not surprisingly, heaving is

the dominant power generating mechanism, while pitching power tends to oscillate between positive and negative values throughout the cycle. Likewise power tends to reach peak values as the airfoil is moving near its maximum velocity during either the upstroke or downstroke portion of the cycle. Aperiodic timevarying modes with frequencies greater than the cycle frequency are apparent in the power output. These are indicative of vortex shedding events, and lead to small cycle-to-cycle variations in power output. For several operating parameter combinations (e.g. Fig. 11(a)), it is apparent that negative power generation occurs over some portion of the cycle. However, cycle-averaged power is positive for all parameter combinations except for that shown in Fig. 11(e), which operates at the highest reduced frequency and pitching amplitude simulated in this study.

The total work on the foil is obtained by integrating power over time:

$$W_{total}(t) = \int_0^t P(\tau) d\tau \tag{7}$$

The integral in Eq. (7) was evaluated over the last 10 cycles of each simulation to determine the efficiency for each set of operating conditions. Tables 1-4 show the predicted efficiencies for each combination of heaving amplitude, pitching amplitude, and reduced frequency. The maximum predicted efficiency of 0.329 occurred for the case with k = 0.14, $h_0 = 0.6$, and $\theta = 75^{\circ}$.

Trends are more easily discernable when efficiency results are presented graphically in Figs. 12-15. It is observed that, for a given combination of heaving and pitching amplitude, the efficiency increases with increasing reduced frequency until a maximum is reached, then decreases as reduced frequency continues to increase. The rate of decrease after the critical value of reduced frequency depends on the other operating conditions. For the range of parameters investigated, the heaving amplitude appears to play the primary role in determining this rate of decrease. As seen for example in Fig. 15, showing results for the highest heaving amplitude of 0.8, once the maximum efficiency is reached at k = 0.12, the drop off with increased k is quite rapid. Overall this suggests that OFEH operation is in general expected to be less robust for systems with relatively high heaving amplitudes compared to lower heaving amplitudes. In contrast, for example, Fig. 13 shows that the cases with $h_0 = 0.4$ have a broader peak in efficiency, suggesting they are more likely to provide high performance in environments with time-varying

freestream velocity. It is apparent that optimum OFEH design should consider the breadth of the efficiency peak and the decrease in performance at higher reduced frequencies, in addition to the overall peak efficiency for any particular design.

Table 2. Predicted efficiency for cases with k = 0.1

	Pitching Amplitude			
Heaving				
Amplitude	65°	70°	75°	80°
0.4c	0.227	0.232	0.205	0.19
0.6c	0.268	0.228	0.231	0.211
0.8c	0.272	0.23	0.231	0.216

Table 3. Predicted efficiency for cases with k = 0.12

	Pitching Amplitude			
Heaving				
Amplitude	65°	70°	75°	80°
0.4c	0.265	0.286	0.271	0.27
0.6c	0.314	0.303	0.298	0.29
0.8c	0.304	0.313	0.294	0.295

Table 4. Predicted efficiency for cases with k = 0.14

	Pitching Amplitude			
Heaving				
Amplitude	65°	70°	75°	80°
0.4c	0.314	0.319	0.306	0.297
0.6c	0.293	0.32	0.329	0.322
0.8c	0.275	0.287	0.275	0.274

Table 5. Predicted efficiency for cases with k = 0.16

	Pitching Amplitude			
Heaving				
Amplitude	65°	70°	75°	80°
0.4c	0.288	0.291	0.306	0.308
0.6c	0.262	0.262	0.262	0.238
0.8c	-	-0.229	-	-

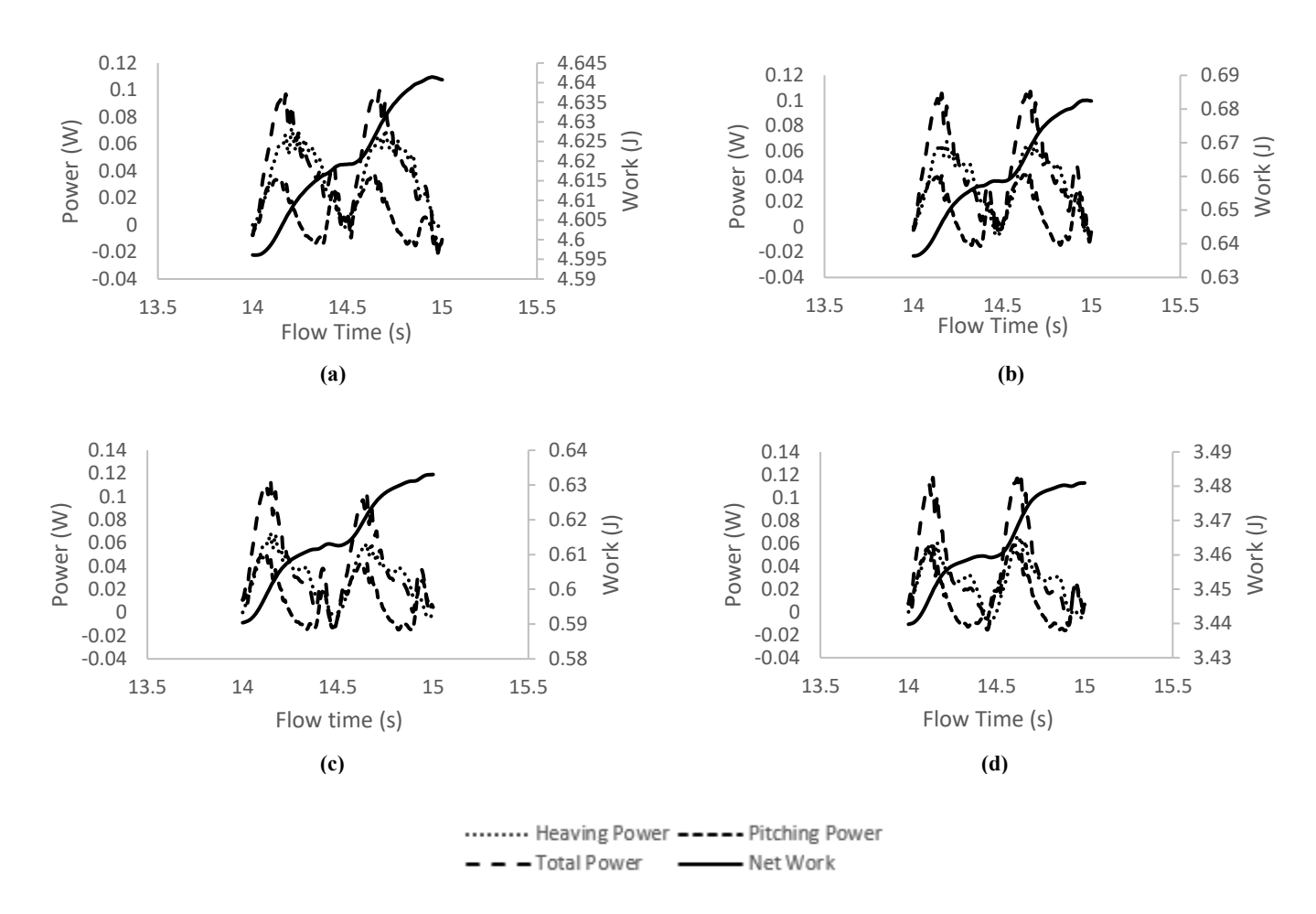


Figure 4. Predicted instantaneous power and total work on foil during one oscillation cycle, (a) k = 0.1, $h_{\theta} = 0.4$, $\theta = 65^{\circ}$, (b) k = 0.1, $h_{\theta} = 0.4$, $\theta = 70^{\circ}$, (c) k = 0.1, $h_{\theta} = 0.4$, $\theta = 75^{\circ}$, (d) k = 0.1, $h_{\theta} = 0.4$, $\theta = 80^{\circ}$.

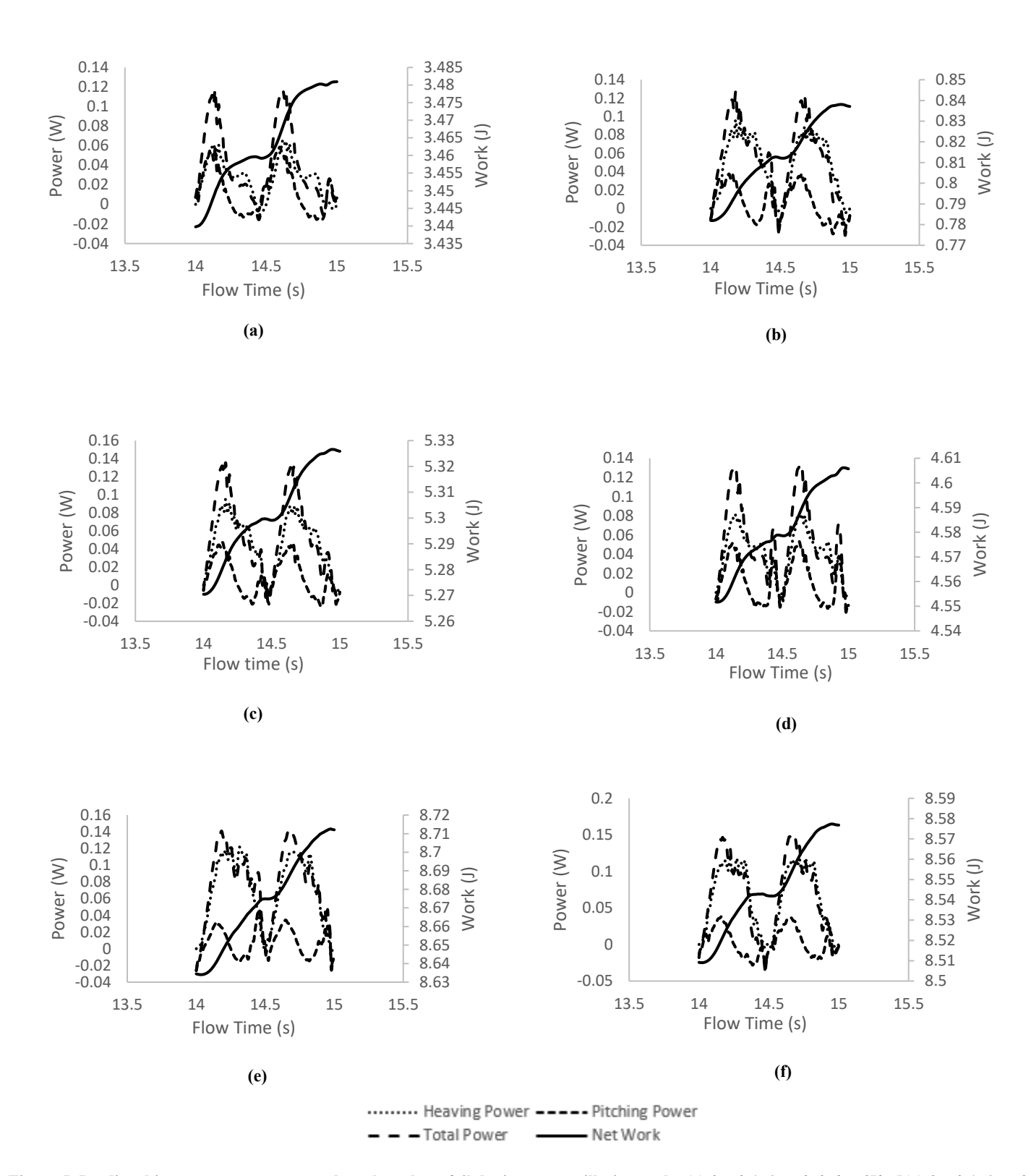


Figure 5. Predicted instantaneous power and total work on foil during one oscillation cycle, (a) k = 0.1, $h_{\theta} = 0.6$, $\theta = 65^{\circ}$, (b)) k = 0.1, $h_{\theta} = 0.6$, $\theta = 70^{\circ}$, (c)) k = 0.1, $h_{\theta} = 0.6$, $\theta = 70^{\circ}$, (d)) k = 0.1, $h_{\theta} = 0.6$, $\theta = 80^{\circ}$, (e)) k = 0.1, $h_{\theta} = 0.8$, $\theta = 65^{\circ}$, (f) k = 0.1, $h_{\theta} = 0.8$, $\theta = 70^{\circ}$.

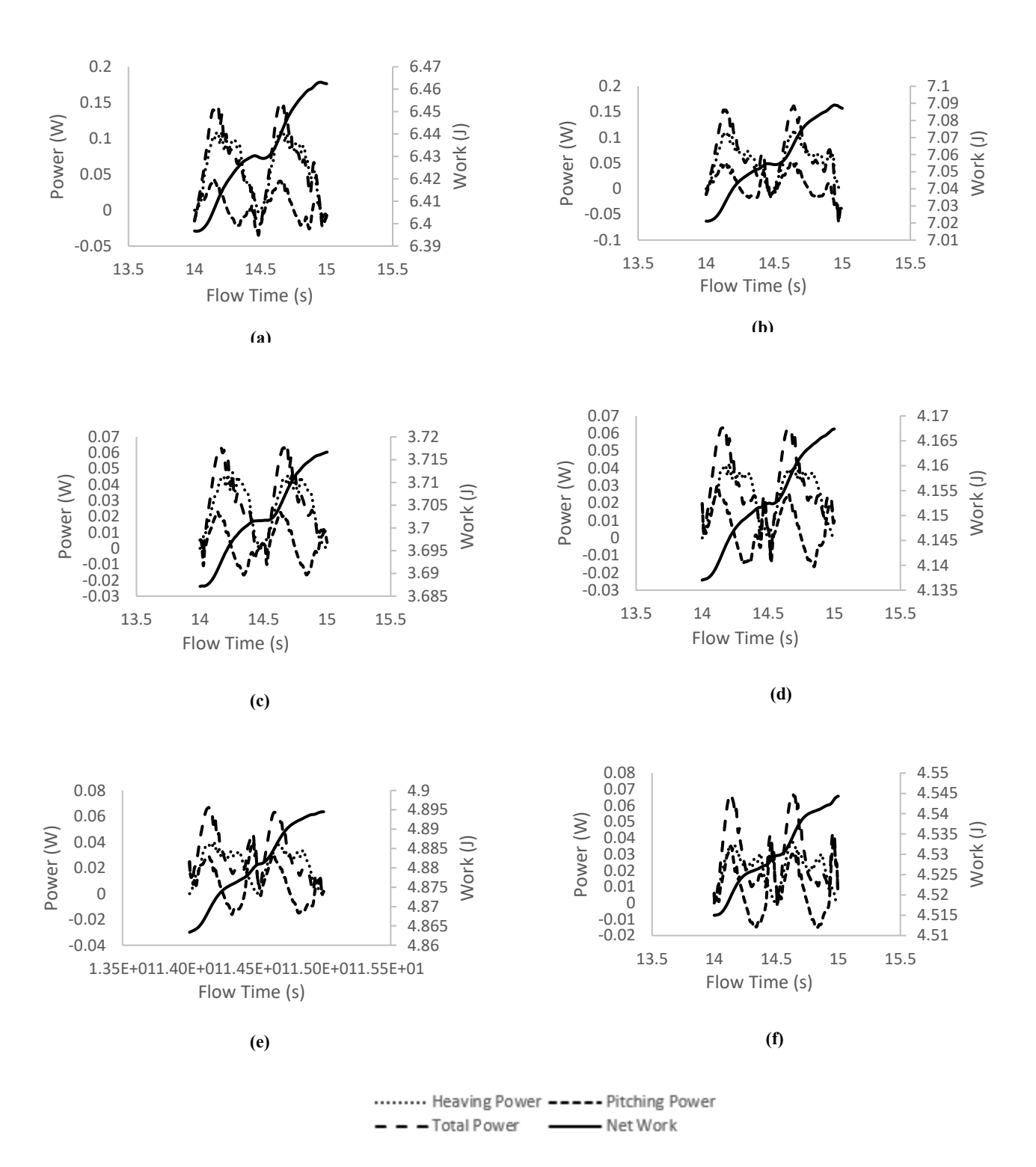


Figure 6. Predicted instantaneous power and total work on foil during one oscillation cycle, (a) k = 0.1, $h_{\theta} = 0.8$, $\theta = 75^{\circ}$, (b) k = 0.1, $h_{\theta} = 0.8$, $\theta = 80^{\circ}$, (c) k = 0.12, $h_{\theta} = 0.4$, $\theta = 65^{\circ}$, (d) k = 0.12, $h_{\theta} = 0.4$, $\theta = 70^{\circ}$, (e) k = 0.12, $h_{\theta} = 0.4$, $\theta = 75^{\circ}$, (f) k = 0.12, $h_{\theta} = 0.4$, $\theta = 80^{\circ}$.

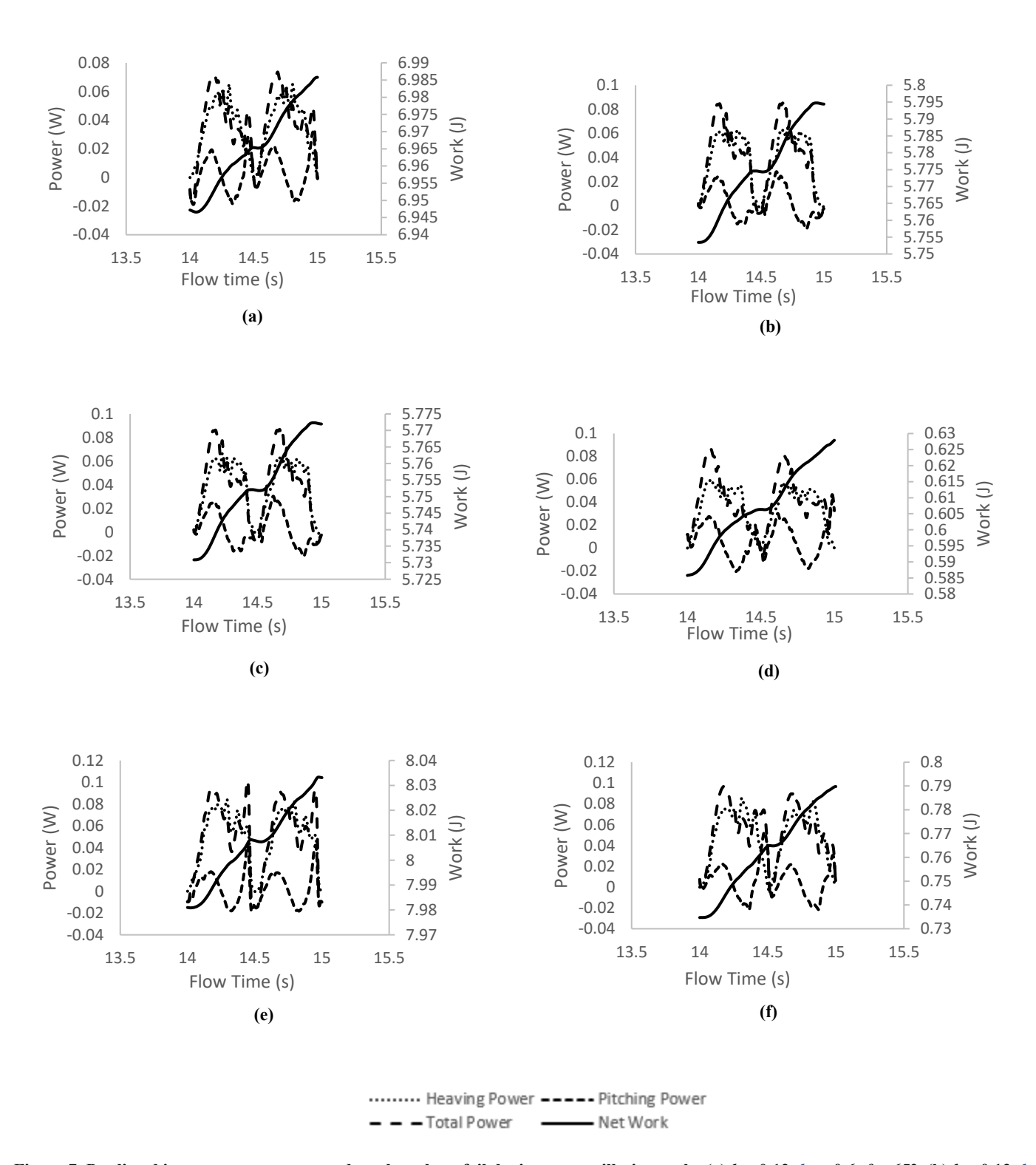


Figure 7. Predicted instantaneous power and total work on foil during one oscillation cycle, (a) k = 0.12, $h_{\theta} = 0.6$, $\theta = 65^{\circ}$, (b) k = 0.12, $h_{\theta} = 0.6$, $\theta = 70^{\circ}$, (c) k = 0.12, $h_{\theta} = 0.6$, $\theta = 75^{\circ}$, (d) k = 0.12, $h_{\theta} = 0.6$, $\theta = 80^{\circ}$, (e) k = 0.12, $h_{\theta} = 0.8$, $\theta = 65^{\circ}$, (f) k = 0.12, $h_{\theta} = 0.8$, $\theta = 70^{\circ}$.

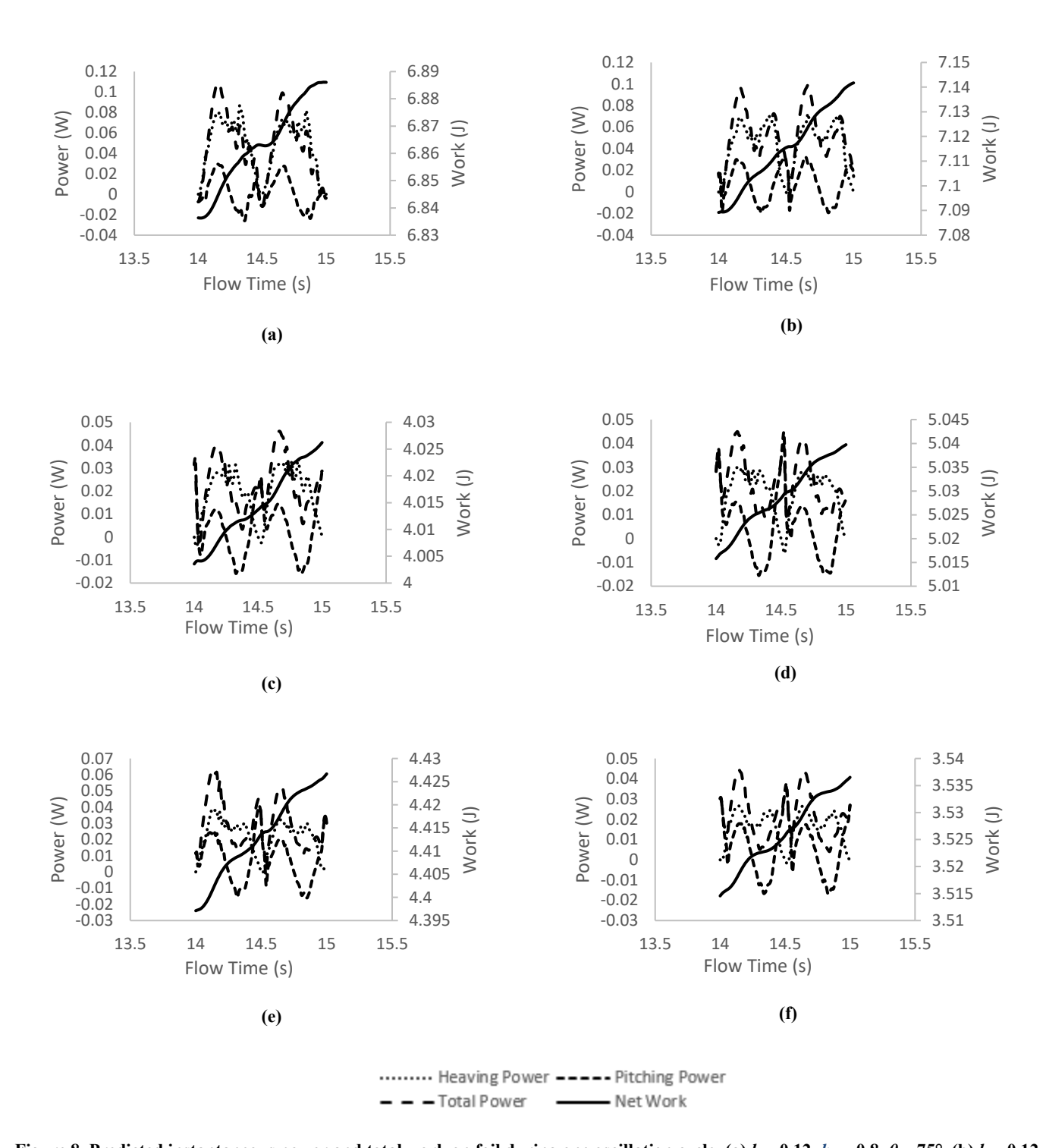


Figure 8. Predicted instantaneous power and total work on foil during one oscillation cycle, (a) k = 0.12, $h_{\theta} = 0.8$, $\theta = 75^{\circ}$, (b) k = 0.12, $h_{\theta} = 0.8$, $\theta = 80^{\circ}$, (c) k = 0.14, $h_{\theta} = 0.4$, $\theta = 65^{\circ}$, (d) k = 0.14, $h_{\theta} = 0.4$, $\theta = 70^{\circ}$, (e) k = 0.14, $h_{\theta} = 0.4$, $\theta = 75^{\circ}$, (f) k = 0.14, $h_{\theta} = 0.4$, $\theta = 80^{\circ}$.

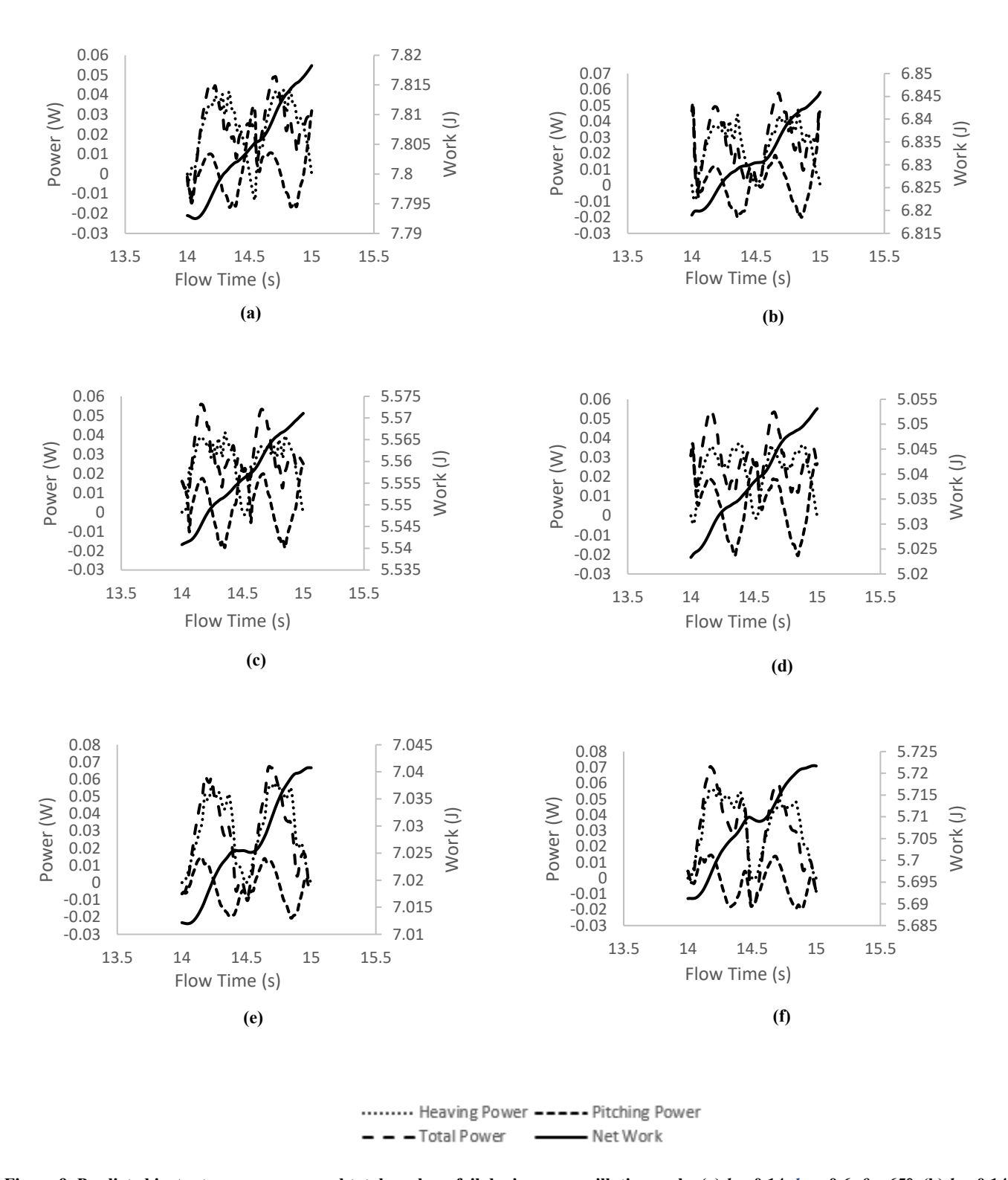


Figure 9. Predicted instantaneous power and total work on foil during one oscillation cycle, (a) k = 0.14, $h_{\theta} = 0.6$, $\theta = 65^{\circ}$, (b) k = 0.14, $h_{\theta} = 0.6$, $\theta = 70^{\circ}$, (c) k = 0.14, $h_{\theta} = 0.6$, $\theta = 70^{\circ}$, (d) k = 0.14, $h_{\theta} = 0.6$, $\theta = 80^{\circ}$, (e) k = 0.14, $h_{\theta} = 0.8$, $\theta = 65^{\circ}$, (f) k = 0.14, $h_{\theta} = 0.8$, $\theta = 70^{\circ}$.

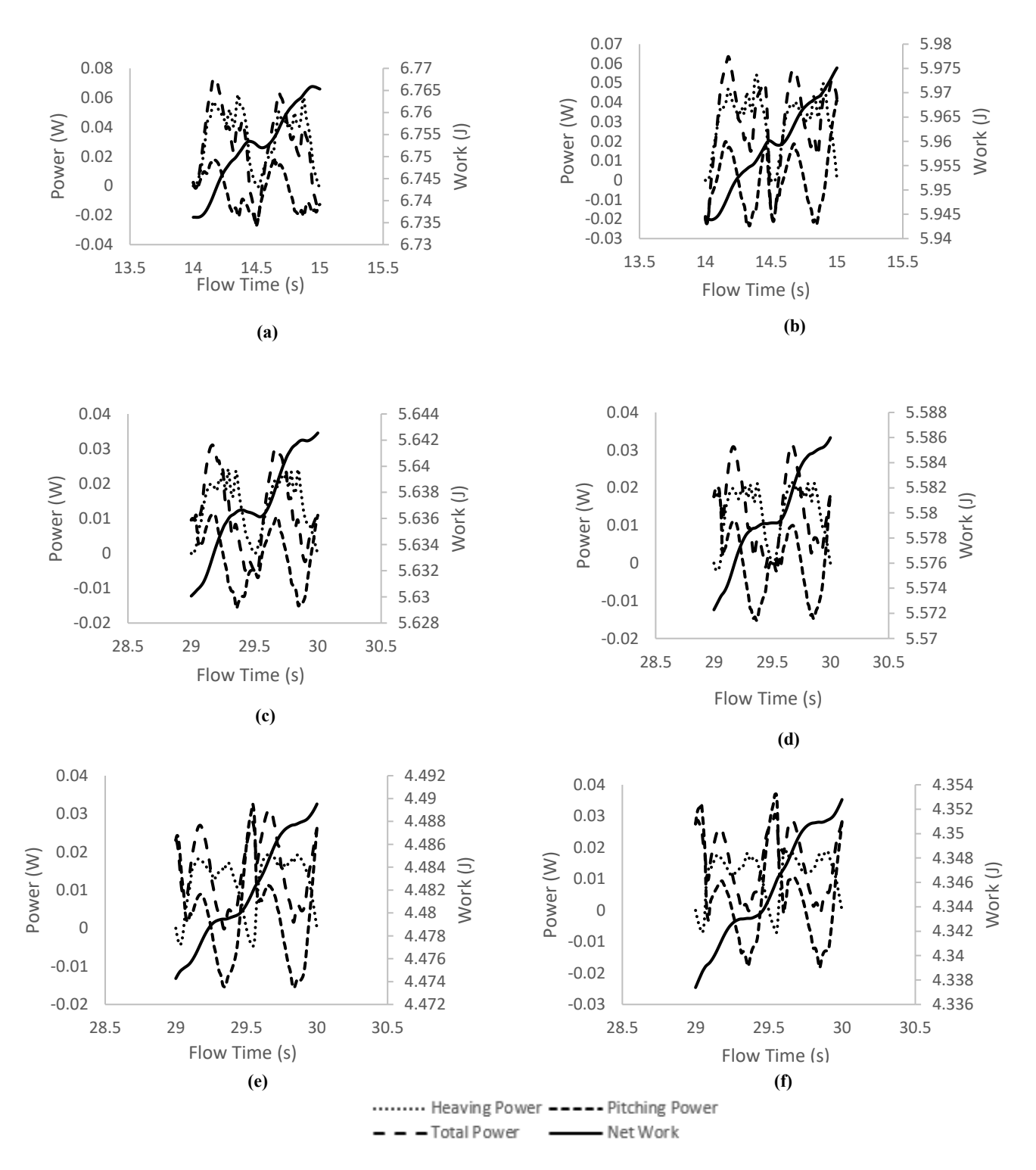


Figure 10. Predicted instantaneous power and total work on foil during one oscillation cycle, (a) k = 0.14, $h_{\theta} = 0.8$, $\theta = 75^{\circ}$, (b) k = 0.14, $h_{\theta} = 0.8$, $\theta = 80^{\circ}$, (c) k = 0.16, $h_{\theta} = 0.4$, $\theta = 65^{\circ}$, (d) k = 0.16, $h_{\theta} = 0.4$, $\theta = 70^{\circ}$, (e) k = 0.16, $h_{\theta} = 0.4$, $\theta = 75^{\circ}$, (f) k = 0.16, $h_{\theta} = 0.4$, $\theta = 80^{\circ}$.

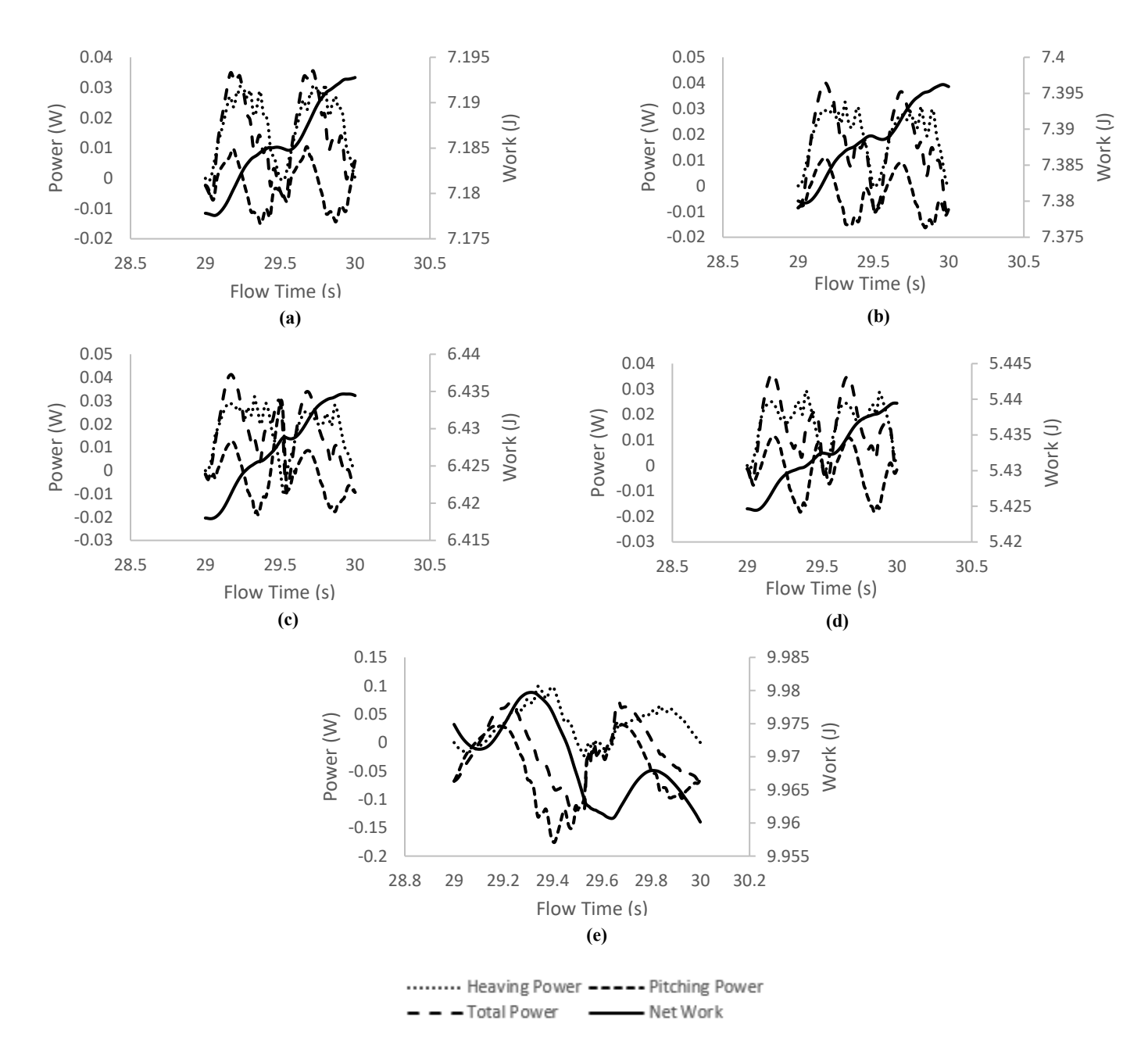


Figure 11. Predicted instantaneous power and total work on foil during one oscillation cycle, (a) k = 0.16, $h_{\theta} = 0.6$, $\theta = 65^{\circ}$, (b) k = 0.16, $h_{\theta} = 0.6$, $\theta = 70^{\circ}$, (c) k = 0.16, $h_{\theta} = 0.6$, $\theta = 75^{\circ}$, (d) k = 0.16, $h_{\theta} = 0.6$, $\theta = 80^{\circ}$, (e) k = 0.16, $h_{\theta} = 0.8$, $\theta = 70^{\circ}$.

Efficiency as a Function of Reduced Frequency Comparisons

Plots of the rate of work due to pitching, rate of work due to heaving, total power, displayed in the figures above reveal several patterns. It seems pitching power is generally a smaller contribution to the total power generation than heaving power. Pitching power always has at least some negative region during the cycle, as the foil rotates against the flow at the top and bottom of heaving motion, and the pitching power seems to bedominated by the frequency of twice the cycle frequency. Oscillations

appear to be almost sinusoidal. In contrast, the heaving power is generally positive, and fluctuates with a smaller amplitude and higher frequency than the pitching power.

The efficiencies of the various cases are also plotted in the following figures. Note that the data seems to indicate that heaving has the greatest role in determining the shape of the efficiency curve.

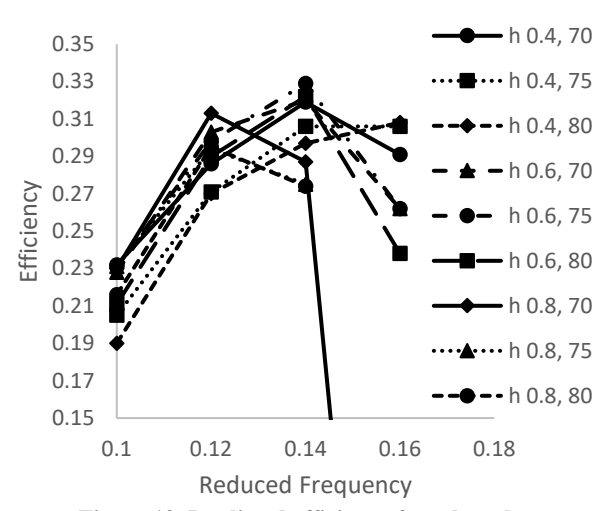


Figure 12. Predicted efficiency for selected cases.

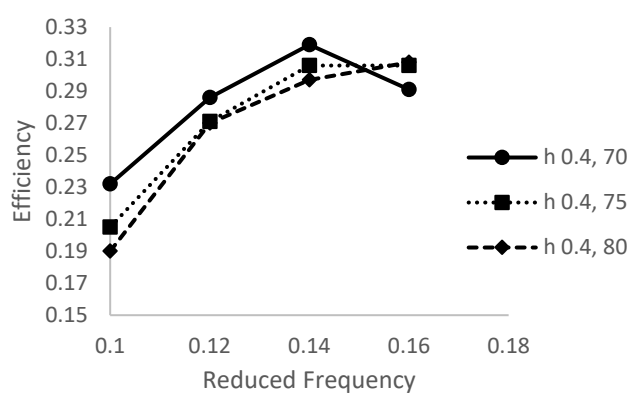


Figure 13. Predicted efficiency for cases with $h_0 = 0.4c$.

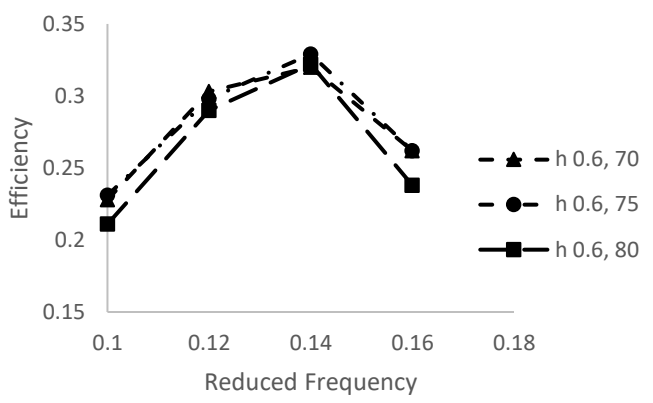


Figure 14. Predicted efficiency for cases with $h_0 = 0.6c$.

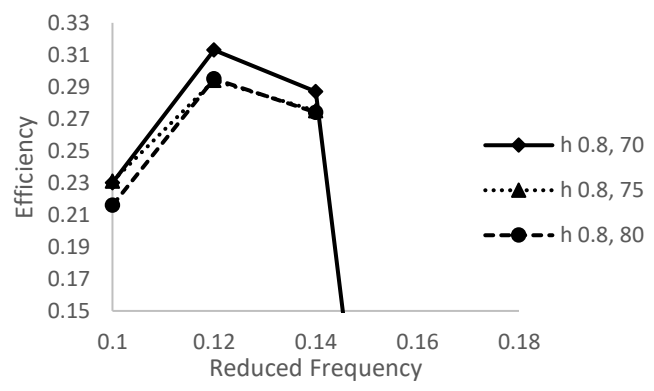


Figure 15. Predicted efficiency for cases with $h_0 = 0.8c$.

VISUALIZATION OF VORTEX SHEDDING

Figure 16 shows vorticity contours at several different times during a single cycle for the case of heaving amplitude 0.6, reduced frequency of 0.12, and pitching amplitude of 75°. The complex shedding behavior is apparent. Of particular significance are times during the cycle when vortices are close to the foil surface, resulting in a significant force contribution due to the low pressure in the vortex core.

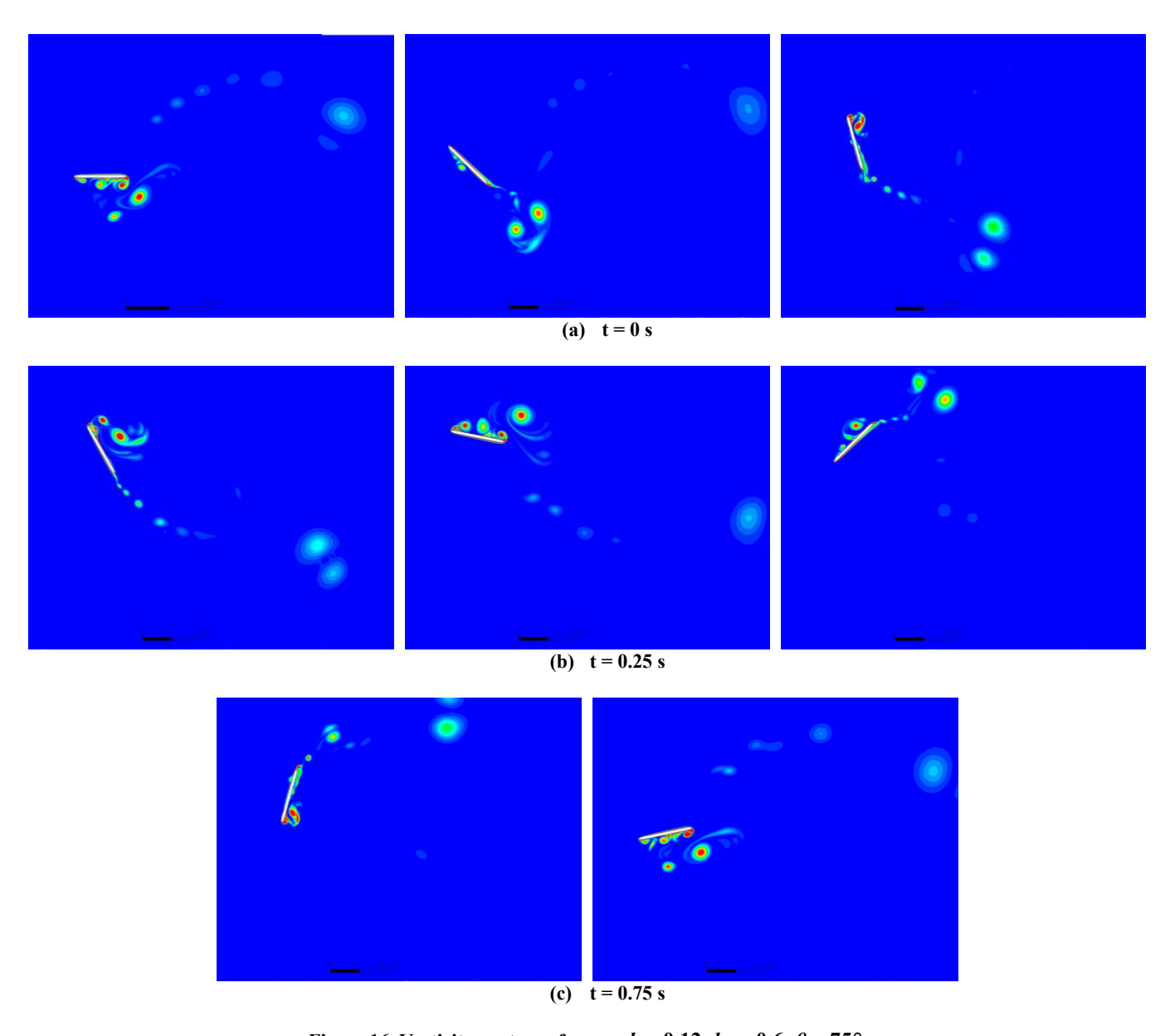


Figure 16. Vorticity contours for case k = 0.12, $h_{\theta} = 0.6$, $\theta = 75^{\circ}$.

CONCLUSIONS

This study investigates the effects of heaving amplitude, pitching amplitude, and reduced frequency on the efficiency of oscillating foil energy harvesters. CFD results using Ansys Fluent indicate that heaving amplitude is the most important factor in determining the behavior of the foil efficiency as a function of reduced frequency. Since heaving and pitching amplitudes can be controlled by designers more easily than reduced frequency, selecting a heaving amplitude which presents a large range of reduced frequencies with high efficiency may be a more effective approach then selecting a design based on maximum overall efficiency.

The simulations reported here will serve as a baseline to investigate novel OFEH design and operation. Future work will potentially investigate flexible airfoils, novel kinematics including multi-mode oscillation cycles, and methods for power take-off dynamics.

ACKNOWLEDGMENTS

This research was funded through National Science Foundation (NSF) Award CBET-1805101. The computing for this project was performed at the OU Supercomputing Center for Education & Research (OSCER) at the University of Oklahoma (OU).

REFERENCES

- [1] Peng, Z., Zhu, Q., 2009, "Energy harvesting through flow-induced oscillations of a foil," American Institute of Physics, Vol. 21, No. 12.
- [2] Kinsey, T. and Dumas, G., 2008, "Parametric study of an oscillating airfoil in a power-extraction regime," AIAA Journal, vol. 46, no. 6, p. 1318.
- [3] Sialas, F. and Liburdy, J., 2020, "Power estimation of flapping foil energy harvesters using vortex impulse theory," Renewable Energy, Vol. 154, pp. 894-902.
- [4] Young, J., Ashraf, M., Lai, J., 2013, "Numerical simulation of fully passive flapping foil power generation," AIAA Journal, Vol. 51, No. 11, pp. 2727 2739.
- [5] Wilcox, D.C. *Turbulence Modeling for CFD*. DCW Industries, Inc., La Canada, California, 1998.
- [6] Walters, D.K. and Cokljat, D., 2008, "A three-equation eddy-viscosity model for Reynolds-averaged Navier-Stokes simulations of transitional flows," *Journal of Fluids Engineering*, 130, No. 121401.